Progress In Electromagnetics Research M, Vol. 41, 1–9, 2015

3D Computation of the Power Lines Magnetic Field

Tonći Modrić*, Slavko Vujević, and Dino Lovrić

Abstract—In this paper, a 3D quasi-static numerical algorithm for computation of the magnetic field produced by power lines is presented. These power lines can be overhead power line phase conductors and shield wires or buried cable line phase conductors. The basis of the presented algorithm is the application of Biot-Savart law and the thin-wire approximation of cylindrical conductors. The catenary form of the power line conductors is approximated by a set of straight cylindrical segments. By summing up contributions of all conductor segments, magnetic field distribution is computed. On the basis of the presented theory, a FORTRAN program PFEMF for computation of the magnetic flux density distribution was developed. For each conductor catenary, it is necessary to define only global coordinates of the beginning and ending points and also the value of the longitudinal phase conductor current. Global coordinates of beginning and ending points of each catenary segment are generated automatically in PFEMF. Numerical results obtained by program PFEMF are compared with results obtained by simple 2D model and results obtained using software package CDEGS.

1. INTRODUCTION

Power frequency (50/60 Hz) magnetic field caused by power lines time-harmonic current is a topic of numerous papers and research studies in the world due to its possible adverse health effects. From the standpoint of public opinion, the worst effects are those of a carcinogenic nature, such as children's leukaemia. The first report, which pointed to a possible correlation between childhood leukaemia and extremely low frequency (ELF) magnetic field, was published in 1979th [1]. Thereafter, a number of epidemiological studies, which have examined the relationship between the aforementioned adverse health effects and magnetic field as the cause, were published [2–5]. In [5], ELF magnetic field is classified as "possibly carcinogenic to humans" (group 2B). The World Health Organisation concludes that "consistent epidemiological evidence suggests that chronic low-intensity ELF magnetic-field exposure is associated with an increased risk of childhood leukaemia", although "the evidence for a causal relationship is limited". The International Commission on Non-Ionizing Radiation Protection (ICNIRP) have assessed the available knowledge and published in 2010 guidelines for limiting exposure to time-varying electric and magnetic fields [6]. According to these guidelines, the reference levels for 50 Hz magnetic flux density are 1000 μT for occupational exposure and 200 μT for general public exposure.

In numerical models for computing power frequency magnetic field, applied methodologies range from the method of moments, finite element method, boundary element method, finite-difference time-domain method, charge simulation method and various hybrid methods. In all these models, the problem is considered as quasi-static [7–9], and therefore attenuation and phase shift of magnetic field are neglected without loss of accuracy.

Simplified 2D models based on the Biot-Savart law are widely used for computation of the overhead power line magnetic field [10–19]. In most of these models, power line conductors satisfy a thin-wire

Received 23 December 2014, Accepted 22 January 2015, Scheduled 24 January 2015

* Corresponding author: Tonći Modrić (tmodric@fesb.hr).

The authors are with the Faculty of Electrical Engineering, Mechanical Engineering and Naval Architecture, University of Split, Rudera Boškovića 32, Split HR-21000, Croatia.

approximation and are treated as infinite line sources positioned at a constant distance from the earth's surface. The number of line sources equals the number of power line conductors and contribution of each conductor is taken into account. Computation of the buried cable lines magnetic field and also different magnetic shielding solutions are presented in [20–24]. In recent years, these 2D models are substituted by more sophisticated 3D models [25–28], which can take the catenary form of power line conductors into account. Consequently, more accurate results of power frequency magnetic field at any point under complex configurations of overhead power lines can be obtained.

In this paper, a 3D quasi-static numerical model for computation of the magnetic field produced by power lines is presented. Power line span conductors are approximated by a set of straight thin-wire cylindrical conductor segments, and time-harmonic current that flows along the conductor axis is approximated by a constant value. Comparison between results of the power lines magnetic flux density distribution obtained by developed 3D model, simplified 2D model and computation module HIFREQ of the CDEGS software package is presented.

The 3D quasi-static numerical model for computation of the magnetic field presented herein is a part of a wider time-harmonic quasi-static electromagnetic model for computation of electric and magnetic field of power lines and substations [29], which is based on the applying finite element technique to an integral equation formulation.

2. POWER LINES GEOMETRICAL MODEL

Various 2D models for computation of the overhead power line magnetic field are presented in [10–19], wherein each power line conductor catenary is approximated by a single thin-wire straight line with average height, parallel to the earth surface. This average height h can be described by following expression:

$$h = h_{\max} - \frac{2}{3} \cdot s \tag{1}$$

where $h_{\max}$ is conductor's maximum height and s the conductors sag.

Since the power line conductors take the form of a catenary, these 2D models are only a rough approximation, and therefore precise computation of the magnetic field, especially when field points are in the vicinity of the power line, is not possible. Besides these analytical and numerical 2D models [10–19], some commercial software packages, which are widely used for computation of power lines and substations electromagnetic field, use the same simplified 2D algorithm.

In [18], three 2D algorithms for computing the electric field intensity of a power line are compared: (a) an algorithm that takes into account a short power line and approximates the conductor charge density by a parabola; (b) an algorithm that takes into account a short power line and approximates the conductor charge density by a constant and (c) an algorithm that takes into account an infinite power line and approximates the conductor charge density by a constant.

On the other hand, in 3D algorithms, the catenary form of the overhead power line conductors can be taken into account more precisely. In 3D numerical model, developed for computation of the magnetic field, power line conductors represent sources, which can be in the air or in the earth. These sources, overhead power line phase conductors, shield wires or buried cable line phase conductors, are oriented along the x-axis of the global Cartesian coordinate system (x, y, z). The origin of the selected coordinate system is on the earth's surface and in the middle of the power line section. Computation of the magnetic field is carried out in the y-z plane, perpendicular to the observed power line section (Figure 1).

In [28, 29], a numerical algorithm for segmentation of the overhead power line conductors is shown. Segmentation has to be done for each power line span separately. In the first step, observed conductor of overhead power line span is subdivided into two parts and then each of these parts is subdivided into thin-wire straight segments whose orthogonal projections are equal. The first part of the overhead power line conductor lies between the beginning point $T_b\,(-\ell/2,\, z_b)$ and the lowest point of the catenary curve $T_{\min}\,(u_{\min},\, z_{\min})$, whereas the second part is located between $T_{\min}$ and the ending point $T_e\,(\ell/2,\, z_e)$.

The input data for the conductor segmentation process are global coordinates of the points $T_b\,(x_b,\, y_b,\, z_b)$, $T_e(x_e,\, y_e,\, z_e)$ and height $z_{\min}$ of the lowest point $T_{\min}$. Overhead power line span conductors take the form of a catenary, which is described by cosine function in the local coordinate

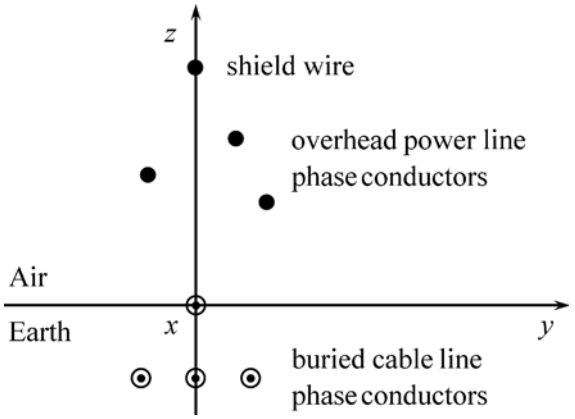

Figure 1. Position of the power line conductors in the global coordinate system.

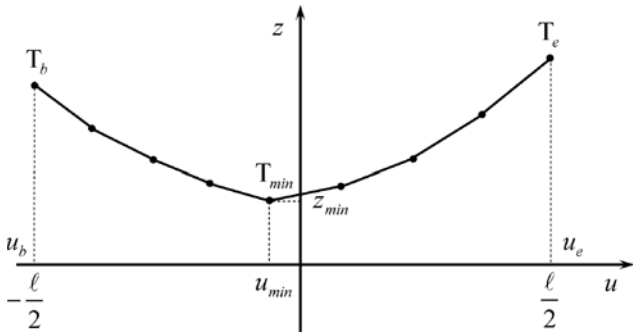

Figure 2. Overhead power line span conductor in the local coordinate system.

system $(u,\, z)$:

$$z = z_{\min} \cdot \cosh \frac{u - u_{\min}}{a} \tag{2}$$

$$a = \frac{\dfrac{\ell}{2} - u_{\min}}{\cosh^{-1} \dfrac{z_e}{z_{\min}}} \tag{3}$$

where ℓ is length of the overhead power line span.

In the general case, the height of the beginning point of the considered overhead power line span conductor z_b is different from the height of the considered ending point z_e (Figure 2).

It was found in [28, 29] that the catenary form of the overhead power line span conductor can be quite accurately approximated by only six straight thin-wire segments, whereas approximation by ten straight segments per overhead power line span conductor can be taken as optimal from a geometrical point of view. However, in electric field intensity computation, a larger number of segments per overhead power line span conductor are required, while in magnetic flux density computation, only accurate approximation of the geometric form of the catenary has to be satisfied.

In the case of buried cable line phase conductors, they have to be divided into straight segments of maximum possible length, parallel to the earth surface. For each segment, it is necessary to define global coordinates of the beginning and ending points and also the value of the longitudinal phase conductor current.

3. COMPUTATION OF THE POWER LINE MAGNETIC FLUX DENSITY

Numerical algorithms for computation of the magnetic flux density of the overhead power line and buried cable line are mathematically identical and are based on the Biot-Savart law. Phasor of the magnetic flux density vector $\underline{\vec{B}}$ at the arbitrary field point $T\,(x,\, y,\, z)$, positioned in the air of the observed two-layer medium consisting of air and earth, is defined by the sum of contributions of all power line conductor segments (NS):

$$\underline{\vec{B}} = \left\{\bar{B}_x, \bar{B}_y, \bar{B}_z\right\} = \sum_{j=1}^{NS} \underline{\vec{B}}_j = \sum_{j=1}^{NS} \frac{\mu_0 \cdot \bar{I}_j}{4 \cdot \pi} \cdot \int\limits_{\Gamma_j} \frac{\mathrm{d}\vec{s}_j \times \vec{R}_j}{R_j^3} \tag{4}$$

where $\bar{B}_x$, $\bar{B}_y$ and $\bar{B}_z$ are the effective (rms) values of the magnetic flux density components, and $\underline{\vec{B}}_j$ is the phasor of the jth cylindrical conductor segment magnetic flux density, $\bar{I}_j$ a phasor of the jth conductor current, Γ_j the integration path positioned along the jth conductor segment axis, R_j the

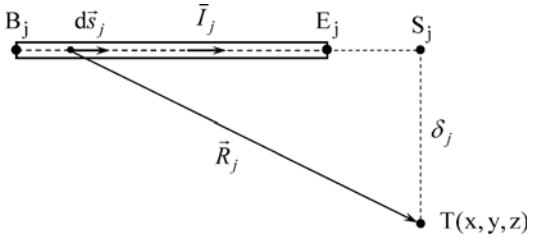

Figure 3. Cylindrical conductor segment.

distance between the point on the jth conductor segment axis and a field point, $\vec{R}_j$ the vector from the point on the jth conductor segment axis and a field point, and μ_0 the vacuum magnetic permeability.

Segment of the jth cylindrical conductor between beginning point B_j and ending point E_j with the longitudinal current $\bar{I}_j$, which is approximated by a constant value and flows along the conductor axis from the beginning point to the ending point, is shown in Figure 3.

According to (4), the following expression can be obtained:

$$\underline{\vec{B}}_j = \frac{\mu_0 \cdot \bar{I}_j \cdot \ell_j}{4 \cdot \pi \cdot \delta_j} \cdot \left[\frac{t_j}{|\vec{r} - \vec{r}_{B_j}|} + \frac{1 - t_j}{|\vec{r} - \vec{r}_{E_j}|} \right] \cdot \vec{d}_{0j} \tag{5}$$

where ℓ_j is the length of the jth cylindrical conductor segment, δ_j the shortest distance between the field point and a path on which lies the jth conductor segment axis, $\vec{r}$ the vector of the field point T, $\vec{r}_{B_j}$ the vector of the beginning point, $\bar{r}_{E_j}$ the vector of the ending point, $\vec{d}_{0j}$ the unit vector of the magnetic flux density of the jth cylindrical conductor segment, and t_j the auxiliary parameter.

The length of the jth cylindrical conductor segment is described by the following expressions:

$$\ell_j = \sqrt{a_j^2 + b_j^2 + c_j^2} \tag{6}$$

$$a_j = x_{E_j} - x_{B_j}; \quad b_j = y_{E_j} - y_{B_j}; \quad c_j = z_{E_j} - z_{B_j} \tag{7}$$

where $(x_{B_j},\, y_{B_j},\, z_{B_j})$ and $(x_{E_j},\, y_{E_j},\, z_{E_j})$ are the global coordinates of the beginning and ending points of the jth cylindrical conductor segment.

The auxiliary parameter t_j from (5) is described by:

$$t_j = \frac{a_j \cdot (x - x_{B_j}) + b_j \cdot (y - y_{B_j}) + c_j \cdot (z - z_{B_j})}{\ell_j^2} \tag{8}$$

The shortest distance between the field point $T\,(x,\, y,\, z)$ and a path on which lies the jth conductor segment axis is described by:

$$\delta_j = |\vec{r} - \vec{r}_S| = \sqrt{(x - x_{S_j})^2 + (y - y_{S_j})^2 + (z - z_{S_j})^2} \tag{9}$$

where the global coordinates of the point S_j can be expressed by:

$$S_j \left(x_{S_j}, y_{S_j}, z_{S_j} \right) = S_j \left(x_{B_j} + a_j \cdot t_j, y_{B_j} + b_j \cdot t_j, z_{B_j} + c_j \cdot t_j \right) \tag{10}$$

The unit vector of the magnetic flux density of the jth cylindrical conductor segment is described by:

$$\vec{d}_{0_j} = \frac{\begin{vmatrix} \vec{i} & \vec{j} & \vec{k} \\ a_j & b_j & c_j \\ x - x_{S_j} & y - y_{S_j} & z - z_{S_j} \end{vmatrix}}{\ell_j \cdot \delta_j} \tag{11}$$

where $\vec{i}$, $\vec{j}$, $\vec{k}$ are unit vectors of the global Cartesian coordinate system.

According to (4)–(11), phasor of the magnetic flux density vector can be obtained by:

$$\underline{\vec{B}}_j = \mu_0 \cdot \frac{\bar{I}_j}{4 \cdot \pi \cdot \delta_j^2} \cdot \left[\frac{t_j}{\left|\vec{r} - \vec{r}_{B_j}\right|} + \frac{1 - t_j}{\left|\vec{r} - \vec{r}_{E_j}\right|} \right] \cdot \begin{vmatrix} \vec{i} & \vec{j} & \vec{k} \\ a_j & b_j & c_j \\ x - x_{S_j} & y - y_{S_j} & z - z_{S_j} \end{vmatrix} \tag{12}$$

The components of the magnetic flux density can be obtained by following expressions:

$$\bar{B}_{jx} = \mu_0 \cdot \frac{\bar{I}_j}{4 \cdot \pi \cdot \delta_j^2} \cdot \left[\frac{t_j}{\left|\vec{r} - \vec{r}_{B_j}\right|} + \frac{1 - t_j}{\left|\vec{r} - \vec{r}_{E_j}\right|} \right] \cdot \left[\left(z - z_{S_j}\right) \cdot b_j - \left(y - y_{S_j}\right) \cdot c_j \right] \tag{13}$$

$$\bar{B}_{jy} = \mu_0 \cdot \frac{\bar{I}_j}{4 \cdot \pi \cdot \delta_j^2} \cdot \left[\frac{t_j}{\left|\vec{r} - \vec{r}_{B_j}\right|} + \frac{1 - t_j}{\left|\vec{r} - \vec{r}_{E_j}\right|} \right] \cdot \left[\left(x - x_{S_j}\right) \cdot c_j - \left(z - z_{S_j}\right) \cdot a_j \right] \tag{14}$$

$$\bar{B}_{jz} = \mu_0 \cdot \frac{\bar{I}_j}{4 \cdot \pi \cdot \delta_j^2} \cdot \left[\frac{t_j}{\left|\vec{r} - \vec{r}_{B_j}\right|} + \frac{1 - t_j}{\left|\vec{r} - \vec{r}_{E_j}\right|} \right] \cdot \left[\left(y - y_{S_j}\right) \cdot a_j - \left(x - x_{S_j}\right) \cdot b_j \right] \tag{15}$$

Finally, the total effective (rms) value of the magnetic flux density at the arbitrary field point $T\,(x,\, y,\, z)$ can be computed using the following expression:

$$B = \sqrt{\left|\bar{B}_x\right|^2 + \left|\bar{B}_y\right|^2 + \left|\bar{B}_z\right|^2} \tag{16}$$

4. NUMERICAL EXAMPLE

Results of the power line magnetic flux density distribution obtained by presented 3D model are compared with results obtained by simplified 2D model and with results obtained using computation module HIFREQ of the CDEGS software package.

For this purpose, a typical 400 kV overhead power line with three phases (L1, L2 and L3), with two conductors in the bundle per phase, and two shield wires (SW1 and SW2) in the horizontal disposition was chosen (Figure 4). Phase conductors are of type AlFe 490/65 mm^2, whereas the shield wires are of type AlMgFe 170/70. This yields the radii of phase conductors $r = 15.30$ mm and radii of shield wires $r = 9$ mm. Power line frequency $f = 50$ Hz, length of the power line section $\ell = 300$ m, relative permittivity of earth $\varepsilon_r = 10$ and electrical conductivity $\sigma = 0.1$ S/m are input data for this numerical

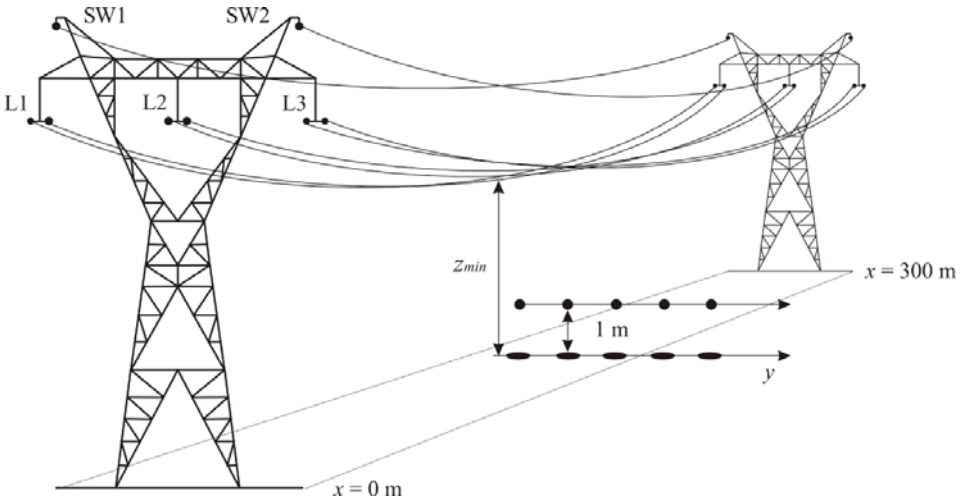

Figure 4. 400 kV overhead power line.

Table 1. Input data of the 400 kV power line.

	i	y (m)	$z_{\max}$ (m)	$z_{\min}$ (m)	$\bar{\varphi}$ (kV)	$\bar{I}$ (A)
L1	1	−10.2	20.0	12.5	$231\angle 0°$	$960\angle -30°$
	2	−9.8	20.0	12.5	$231\angle 0°$	$960\angle -30°$
L2	3	−0.2	20.0	12.5	$231\angle -120°$	$960\angle -150°$
	4	0.2	20.0	12.5	$231\angle -120°$	$960\angle -150°$
L3	5	9.8	20.0	12.5	$231\angle 120°$	$960\angle 90°$
	6	10.2	20.0	12.5	$231\angle 120°$	$960\angle 90°$
SW1	7	−6.0	23.7	16.2	$0\angle 0°$	$0\angle 0°$
SW2	8	6.0	23.7	16.2	$0\angle 0°$	$0\angle 0°$

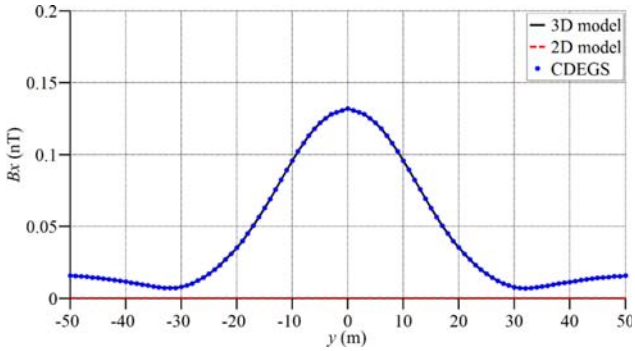

Figure 5. Effective values of the x-component of the magnetic flux density.

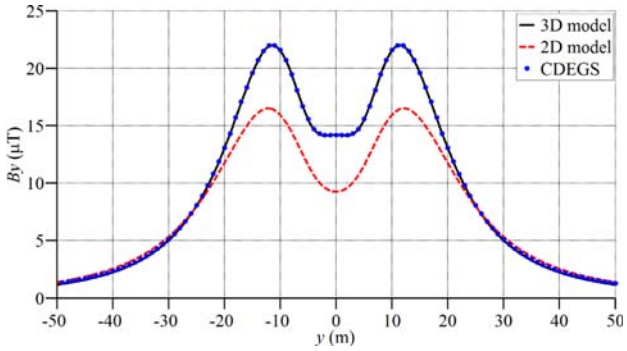

Figure 6. Effective values of the y-component of the magnetic flux density.

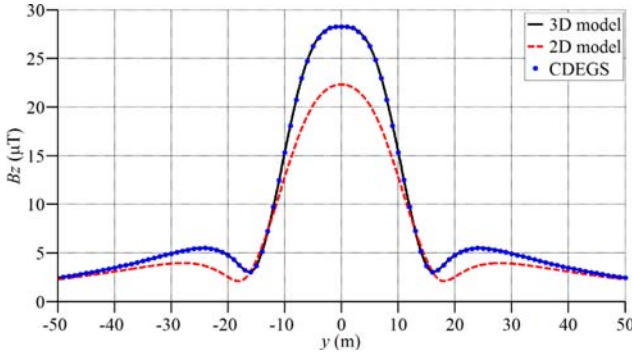

Figure 7. Effective values of the z-component of the magnetic flux density.

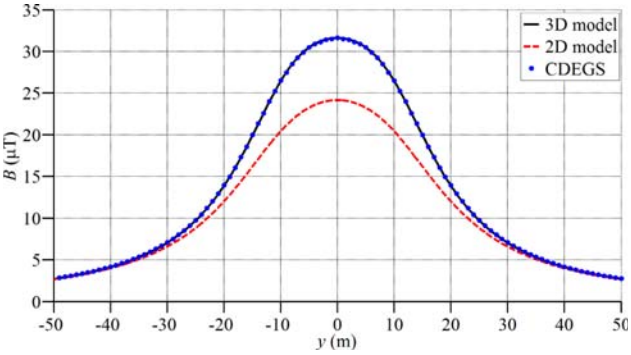

Figure 8. Effective values of the total magnetic flux density.

example. Other electrical and geometrical input data are given in Table 1. Besides these data, it is also necessary to specify the total number of segments in which it should be divided each catenary. It is assumed that the maximum allowed conductor current is flowing through the phase conductor, although this is not the case in most circumstances. Moreover, symmetrical operating conditions have been assumed. Despite this, a 3D algorithm described in this paper can also be used in a case of non-symmetrical operating conditions (e.g., single-pole short circuits).

On the basis of the presented theory, a FORTRAN program PFEMF (Power Frequency ElectroMagnetic Field) was developed. Computation of the magnetic flux density distribution is carried out at midspan along the y-directed (lateral) profile, 1 m above the earth's surface (i.e., $z = 1$ m). The

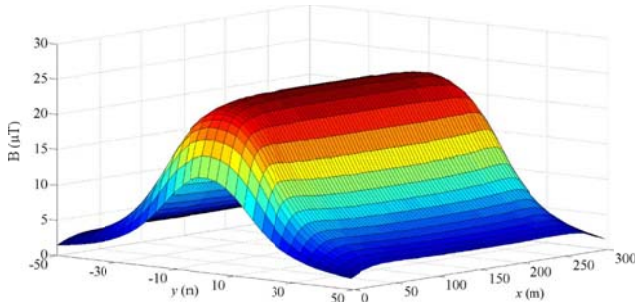

Figure 9. Spatial distribution of the magnetic flux density computed using 2D model.

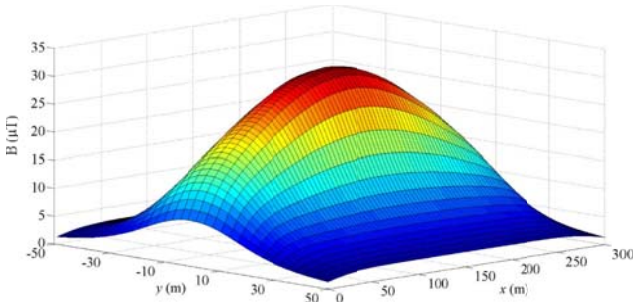

Figure 10. Spatial distribution of the magnetic flux density computed using 3D model.

$z_{\min}$ values in Table 1 represent minimum heights of the overhead power line conductors, which are, due to symmetry and equal heights of both towers, positioned at midspan. In this example, the height of the beginning (z_b) and ending point (z_e) of the considered overhead power line span are equal ($z_b = z_e = z$), as well as the conductor's sag ($s = 7.5\,\text{m}$). For each segment, global coordinates of the beginning and ending points of the each catenary are generated automatically in PFEMF. In the computation module HIFREQ of the CDEGS software package, assignment of input data requires much more time.

Figures 5–8 present computed effective values of the magnetic flux density components and total effective values of the magnetic flux density distribution along the observation profile.

By comparing the obtained results of the magnetic flux density distribution, a substantial influence of taking into account the actual shape of the power line conductor's catenary is shown. This is most apparent at midspan where the conductor's sag is the greatest. The largest percent error of the total magnetic flux density between presented 3D model and CDEGS software package is 0.06%. The largest percent error between 3D model and simplified 2D model [18] with the revised average heights of the conductors is 23.6%.

Spatial distribution of the total magnetic flux density obtained by simplified 2D model and advanced 3D model (using PFEMF and CDEGS) are shown in Figures 9 and 10.

Computation of the magnetic flux density using 3D models is obviously more accurate than using 2D models, but often requires long computation time. That is not a case herein, with presented algorithm and PFEMF program. Results obtained by computation module HIFREQ of the widely used CDEGS software package are identical to the results obtained by presented 3D model, but computation time is substantially different. In the selected simple numerical example, computation time of the magnetic flux density spatial distribution in 301 points along the x-axis and 101 points along the y-axis, i.e., totally 30401 points, with PFEMF was only 5 s. The same computation in the module HIFREQ of the CDEGS software package lasted over 500 s.

The possible health effects of exposure to magnetic field have been extensively discussed in numerous epidemiological studies, some of which are listed in [2–5]. Results of the power line magnetic flux density distribution, presented in Figures 5–10, in the vicinity of the 400 kV overhead power line obtained with the maximum allowed conductor currents flowing through the phase conductors, can be compared to ICNIRP guidelines [6]. Computed maximum value of the magnetic flux density right below the lowest point of the power line span conductor is equal to 31.65 μT, which is substantially less than the exposure limits specified by international guidelines [6]. By increasing the distance from the observed power lines, effective values of the magnetic flux density are significantly reduced.

Although various 3D algorithms for computation of the power lines magnetic field are based on the Biot-Savart law [25–27], there are certain differences between them and algorithm presented herein. In [25–27], the exact shape of the catenary is taken into account and in order to compute all the components and the total magnetic flux density, numerical integration of the complex functions have to be done. This is required for each power line conductor's catenary which leads to long computation time and much more complicated mathematical model then model presented in this paper. Therefore, in [26], catenary approximation by a set of straight segments is mentioned as an alternative solution. This approach is used in this paper, and with a simple mathematical model, sufficiently accurate results as it is considered a real catenary form, were obtained.

5. CONCLUSION

A 3D quasi-static numerical algorithm for computation of the power lines magnetic field is presented. The sources of the magnetic field are conductor currents, which are input data for the computation. The catenary form of the power line conductors is approximated by straight segments and contributions of all these segments to the magnetic field are taken into account.

The accuracy of the developed 3D quasi-static algorithm is confirmed in numerical example of 400 kV overhead power line, comparing the obtained results with results obtained by computation module HIFREQ of the CDEGS software package. More accurate results of the magnetic flux density distribution are obtained using this 3D model instead of 2D models. Moreover, assignment of input data is much easier and computation time was significantly shorter than in the CDEGS software package.

The presented algorithm, based on the thin-wire approximation of cylindrical conductors, is only a part of a wider time-harmonic quasi-static electromagnetic model for electric and magnetic field computation of power lines and substations. In a wider electromagnetic model, the influence of overhead power line towers on magnetic field distribution can be taken into account using a set of inductively coupled current contours. However, obtained numerical results indicate that this influence can be neglected.

REFERENCES

1. Wertheimer, N. and E. Leeper, "Electrical wiring configurations and childhood cancer," *American Journal of Epidemiology*, Vol. 109, No. 3, 273–284, 1979.
2. Savitz, D. A. and D. P. Loomis, "Magnetic field exposure in relation to leukemia and brain cancer mortality among electric utility workers," *American Journal of Epidemiology*, Vol. 141, No. 2, 123–134, 1995.
3. Verkasalo, P. K., "Magnetic fields and leukemia-risk for adults living close to power lines," *Scandinavian Journal of Work, Environment & Health*, Vol. 22, No. 2, 1–56, 1996.
4. Kroll, M. E., J. Swanson, T. J. Vincent, and G. J. Draper, "Childhood cancer and magnetic fields from high-voltage power lines in England and Wales: A case-control study," *British Journal of Cancer*, Vol. 103, No. 7, 1122–1127, 2010.
5. IARC, "Non-ionizing radiation, Part 1: Static and extremely low-frequency (ELF) electric and magnetic fields," *IARC Monographs on the Evaluation of Carcinogenic Risks to Humans*, Vol. 80, 1–395, 2002.
6. International Commission on Non-ionizing Radiation Protection, "Guidelines for limiting exposure to time-varying electric and magnetic fields (1 Hz to 100 kHz)," *Health Physics*, Vol. 99, No. 6, 818–836, 2010.
7. Haznadar, Z. and Ž. Štih, *Electromagnetic Fields, Waves and Numerical Methods*, IOS Press, Amsterdam, 2000.
8. Fitzpatrick, R., *Maxwell's Equations and the Principles of Electromagnetism*, Infinity Science Press LLC, Hingham, 2008.
9. Olsen, R. G. and P. S. Wong, "Characteristics of low frequency electric and magnetic fields in the vicinity of electric power lines," *IEEE Transactions on Power Delivery*, Vol. 7, No. 4, 2046–2055, 1992.
10. Moro, F. and R. Turri, "Fast analytical computation of power-line magnetic fields by complex vector method," *IEEE Transactions on Power Delivery*, Vol. 23, No. 2, 1042–1048, 2008.
11. Kaune, W. T. and L. E. Zaffanella, "Analysis of magnetic fields produced far from electric power lines," *IEEE Transactions on Power Delivery*, Vol. 7, No. 4, 2082–2091, 1992.
12. Memari, A. R. and W. Janischewskyj, "Mitigation of magnetic field near power lines," *IEEE Transactions on Power Delivery*, Vol. 11, No. 3, 1577–1586, 1996.
13. Filippopoulos, G. and D. Tsanakas, "Analytical calculation of the magnetic field produced by electric power lines," *IEEE Transactions on Power Delivery*, Vol. 20, No. 2, 1474–1482, 2005.

14. Garrido, C., A. F. Otero, and J. Cidrás, "Low-frequency magnetic fields from electrical appliances and power lines," *IEEE Transactions on Power Delivery*, Vol. 18, No. 4, 1310–1319, 2003.
15. Olsen, R. G., D. Deno, R. S. Baishiki, et al., "Magnetic fields from electric power lines theory and comparison to measurements," *IEEE Transactions on Power Delivery*, Vol. 3, No. 4, 2127–2136, 1988.
16. Ranković, V. and J. Radulović, "Prediction of magnetic field near power lines by normalized radial basis function network," *Advances in Engineering Software*, Vol. 42, No. 11, 934–938, 2011.
17. Vujević, S., P. Sarajčev, and D. Lovrić, "Computation of the power line electric and magnetic fields," *Proceedings of the 17th Telecommunications Forum TELFOR*, 875–878, Belgrade, Serbia, Nov. 2009.
18. Vujević, S., D. Lovrić, and P. Sarajčev, "Comparison of 2D algorithms for the computation of power line electric and magnetic fields," *European Transactions on Electrical Power*, Vol. 21, No. 1, 505–521, 2011.
19. Ismail, H. M., "Characteristics of the magnetic field under hybrid AC/DC high voltage transmission lines," *Electric Power Systems Research*, Vol. 79, No. 1, 1–7, 2009.
20. Habiballah, I. O., A. S. Farag, M. M. Dawoud, and A. Firoz, "Underground cable magnetic field simulation and management using new design configurations," *Electric Power Systems Research*, Vol. 45, No. 2, 141–148, 1998.
21. San Segundo, H. B. and V. F. Roig, "Reduction of low voltage power cables electromagnetic field emission in MV/LV substations," *Electric Power Systems Research*, Vol. 78, No. 6, 1080–1088, 2008.
22. Almeida, M. E., V. M. Machado, and M. G. Das Neves, "Mitigation of the magnetic field due to underground power cables using an optimized grid," *European Transactions on Electrical Power*, Vol. 21, No. 1, 180–187, 2011.
23. Machado, V. M., "Magnetic field mitigation shielding of underground power cables," *IEEE Transactions on Magnetics*, Vol. 48, No. 2, 707–710, 2012.
24. Canova, A., D. Bavastro, F. Freschi, L. Giaccone, and M. Repetto, "Magnetic shielding solutions for the junction zone of high voltage underground power lines," *Electric Power Systems Research*, Vol. 89, 109–115, 2012.
25. El Dein, A. Z., "Magnetic-field calculation under EHV transmission lines for more realistic cases," *IEEE Transactions on Power Delivery*, Vol. 24, No. 4, 2214–2222, 2009.
26. Lucca, G., "Magnetic field produced by power lines with complex geometry," *European Transactions on Electrical Power*, Vol. 21, No. 1, 52–58, 2011.
27. Salari, J. C., A. Mpalantinos, and J. I. Silva, "Comparative analysis of 2- and 3-D methods for computing electric and magnetic fields generated by overhead transmission lines," *IEEE Transactions on Power Delivery*, Vol. 24, No. 1, 338–344, 2009.
28. Modrić, T., S. Vujević, and T. Majić, "Geometrical approximation of the overhead power line conductors," *International Review on Modelling and Simulations*, Vol. 7, No. 1, 76–82, 2014.
29. Modrić, T., "Advanced numerical computation of electromagnetic field of power lines and substations," Ph.D. Thesis, University of Split, FESB, 2014 (in Croatian).